Violating Bell's Inequality using Polarization Entangled Photons

Nathan Ormsby, Gabriel Hain

April 2023

1 Abstract

This capstone is to design and build the experiment to violate Bell's Inequality using polarization-entangled photons. A 405 nanometer (nm) laser is pumped through a Type 1 Beta Barium Borate (BBO) crystal, where a tiny fraction of the pump photons undergo spontaneous parametric down conversion (SPDC). SPDC splits a single photon into an entangled pair of photons, consisting of a signal photon and an idler photon. These photons are entangled such that their polarizations are identical: if the polarization of one photon is measured, then the other is known with certainty. In addition, their paths are deflected at 3° to the incident beam, and their wavelengths are doubled. To test whether Bell's inequality is violated, a pair of linear polarizers in the paths of these entangled photons are moved through polarization differences with respect to one another, and the coincident detection counts of the entangled photons are recorded. A calculation can then be made to test the classical constraint of the CHSH (Clauser, Horne, Shimony, Holt) interpretation of the Bell Inequality, which is the Bell's Inequality relevant to this experiment. [8] If the classical constraint of CHSH is violated, it will mean that this experiment has successfully disproved the existence of hidden variables, and proved the existence of superposition of unobserved particles.

2 Introduction

The idea that the nature of reality cannot be determined until it is observed is a controversial and fundamental principle of quantum mechanics. In 1927, Albert Einstein and his colleagues proposed the Theory of Hidden Variables, which posited that particles were in definite states at all times, rather than in a state of superposition when not being observed, due to some unmeasurable hidden variable. [6] To support their theory, they devised a thought experiment named the EPR Paradox that demonstrated information appeared to travel faster than the speed of light when two entangled particles were separated by a large distance, one particle was measured, and the state of the other particle collapsed instantly. Einstein argued that the only way to explain this phenomenon without violating special relativity was to conclude that the entangled particles were in definite states the entire time, and that a hidden variable existed that determined which particle received which state. This argument was so persuasive that it was considered a valid interpretation of quantum mechanics for nearly 40 years, as no one could devise a method to disprove it.

It wasn't until 1964 that John Stewart Bell developed a mathematical method to determine the validity of the Theory of Hidden Variables. [7] Bell created an inequality that, if broken, would disprove the existence of a hidden variable. He mathematically demonstrated that a purely quantum approach was incompatible with this constraint, effectively invalidating the Theory of Hidden Variables as an interpretation of quantum mechanics and instead solidifying it as an opposing theory. Bell's method was based on the notion that particles in defined states and those in superposition behave differently when measured across different detector configurations. Since then, various interpretations of Bell's Inequality involving different entangled quantities have been formulated and experimental tests have consistently confirmed that reality adheres to quantum mechanics, thereby refuting the existence of hidden variables.

3 Theory

Before a full derivation of the classical constraint, as well as a quantum violation is demonstrated, it is important to justify why the CHSH inequality is the Bell Inequality chosen for this experiment. Along with Bell's original publication, there have been numerous types of Bell's Inequalities published. The primary reason the CHSH Inequality was chosen is because of its simplistic experimental design, and singular type of required measurement. Experiments involving entangled particles of any sort are often delicate and it can be difficult or impossible to perform if there are too many types of detectors needed, or too many types of measurements required by some inequality. This is the primary reason an experiment could not be devised for Bell's original publication in 1964. It wasn't until the CHSH inequality was published in 1969 that an experiment could be designed and later executed. Figure 1 shows an outline of the experimental configuration required by the CHSH inequality.

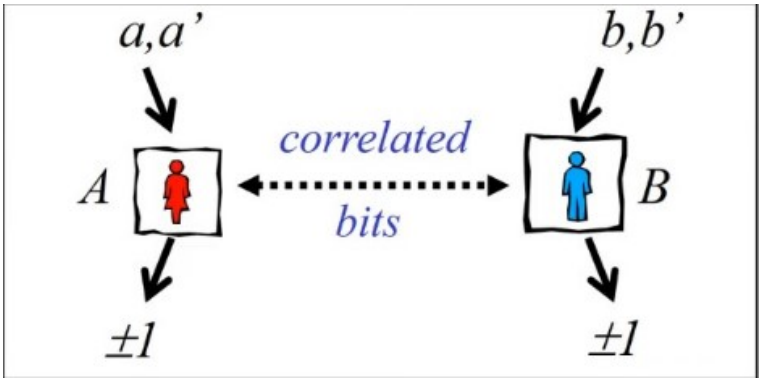

Figure 1: CHSH Configuration

As can be seen in the configuration, in order to perform an experiment violating the CHSH inequality in the laboratory, there are two requirements. First there must be a source of entangled pairs of photons that have identical polarizations, these are the correlated bits. Second there must be configurable detectors that can span several modes capable of measuring the polarization of the entangled photons. The simplest option is a pair of linear polarizers, A and B, that are capable of rotating to respective angles a, a' for polarizer A, and b, b' for polarizer B. The polarizers have outputs of $+1$ if a photon passes through them and -1 if a photon gets blocked. Linear polarizers only allow photons through if they are deemed vertically polarized in the rotated basis of the polarizer. Classically, if a photon passes through a polarizer, it is deemed to hold a value of vertical polarization in that rotated basis. However, the quantum mechanical interpretation differs. Each photon's polarization is defined as some combination of components in both the vertical and horizontal direction in the non rotated basis that when summed together equals its angle of polarization. Thus the photon has a probability of passing through a rotated polarizer that depends on the relation between the angle of the polarizer and the angle of the photon's polarization. It is important to mention the main distinction between these interpretations. Quantum mechanics predicts a random outcome based on some probability of whether a photon passes through the polarizer or not, while the classical interpretation implies that a certain outcome is based on some characteristic of the photon.

The only further requirement is one singular type of measurement, which is that the experimental apparatus must be capable of counting the instances per some period of time when both entangled photons in a single pair pass through their respective polarizers. Now that the CHSH Inequality has been adequately justified in its being chosen for this experimental design, we will now demonstrate a full derivation of the CHSH classical inequality constraint, and how quantum mechanics leads to a violation of this constraint for a particular configuration.

Assuming the validity of the Theory of Hidden Variables and the existence of said hidden variable, measurements made by each polarizer would depend solely on its angle and the hidden variable, which

can be represented by "λ". A probability distribution, $p(\lambda)$ can be made with the conditions $p(\lambda) \geq 0$ and $\int p(\lambda)\,\mathrm{d}\lambda = 1$. Detecting a vertically and horizontally polarized photon may be expressed as $A(\alpha,\, \lambda) = \pm 1$, and $B(\beta,\, \lambda) = \pm 1$ respectively, where α is the angle polarizer "A" is set to, and β is the angle polarizer B is set to.

Since the hidden variable theory posits that the entangled photons exist in a definite state of either horizontal or vertical polarization, rather than a superposition, it becomes possible to express each detectable outcome as an integral of the probability distribution of the hidden variable.

$$
\begin{aligned}
P_{VV} &= \int \left[\frac{1 + A(\alpha, \lambda)}{2} \times \frac{1 + B(\beta, \lambda)}{2}\right] p(\lambda), \mathrm{d}\lambda \\
P_{HH} &= \int \left[\frac{1 - A(\alpha, \lambda)}{2} \times \frac{1 - B(\beta, \lambda)}{2}\right] p(\lambda), \mathrm{d}\lambda \\
P_{VH} &= \int \left[\frac{1 + A(\alpha, \lambda)}{2} \times \frac{1 - B(\beta, \lambda)}{2}\right] p(\lambda), \mathrm{d}\lambda \\
P_{HV} &= \int \left[\frac{1 - A(\alpha, \lambda)}{2} \times \frac{1 + B(\beta, \lambda)}{2}\right] p(\lambda), \mathrm{d}\lambda
\end{aligned}
$$

The subscript of P indicates the polarization direction, with H representing horizontal and V representing vertical for the A and B polarizers, respectively. The number 1 is added as a correction because the output of A or B could potentially be -1, and the probability must always be greater than zero. The denominator of 2 serves to normalize the value, as the integral of the probability distribution must not exceed 1.

A quantity E can be defined in terms of detector outcome probabilities that simplifies elegantly.

$$
E(\alpha, \beta) = P_{VV} + P_{HH} - P_{VH} - P_{HV} = \int A(\alpha, \lambda)\, B(\beta, \lambda)\, p(\lambda)\, \mathrm{d}\lambda \tag{1}
$$

Using the definition of E in (1), the following can be shown in (2).

$$
E(a, b) - E(a, b') = \int \left[A(a, \lambda)\, B(b, \lambda) - A(a, \lambda)\, B(b', \lambda)\right] p(\lambda)\, \mathrm{d}\lambda \tag{2}
$$

Where a, a', b, b' are the aforementioned polarizer angles.

An expression comprising the remaining detector modes will be added and subtracted to the right hand side (RHS) of (2), resulting in (3) being equivalent to (2).

$$
\begin{aligned}
E(a, b) - E(a, b') \;=\; \int \big[&A(a, \lambda)\, B(b, \lambda) - A(a, \lambda)\, B(b', \lambda) \pm A(a, \lambda)\, B(b, \lambda)\, A(a', \lambda)\, B(b', \lambda) \\
&\mp A(a, \lambda)\, B(b, \lambda)\, A(a', \lambda)\, B(b', \lambda)\big]\, p(\lambda)\, \mathrm{d}x
\end{aligned} \tag{3}
$$

The shared terms can be factored from the first and third terms, as well as the second and fourth terms of the RHS of equation (3). This can be expressed as separate integrals, as illustrated in equation (4).

$$
\begin{aligned}
E(a,b) - E(a,b') \;=\; & \int A(a,\lambda)\, B(b,\lambda)[1 \pm A(a',\lambda)\, B(b',\lambda)]\, p(\lambda)\, \mathrm{d}\lambda \\
& - \int A(a,\lambda)\, B(b',\lambda)[1 \pm A(a',\lambda)\, B(b,\lambda)]\, p(\lambda)\, \mathrm{d}\lambda
\end{aligned}
\tag{4}
$$

Upon close examination of the RHS of equation (4), it becomes apparent that all four distinct detector modes (polarizer configurations) are now included. These four modes are (a, b), (a', b), (a, b'), and (a', b').

The triangle inequality, (5), can be applied by taking the absolute value of both sides of (4), as shown in (6).

$$
|x + y| \;\leq\; |x| + |y| \tag{5}
$$

$$
\begin{aligned}
|E(a,\, b) \,-\, E(a,\, b')| \;\leq\; & \Big| \int A(a,\lambda)\, B(b,\lambda)[1 \pm A(a',\lambda)\, B(b',\lambda)]\, p(\lambda)\, \mathrm{d}\lambda \Big| \\
& + \Big| \int A(a,\lambda)\, B(b',\lambda)[1 \pm A(a',\lambda)\, B(b,\lambda)]\, p(\lambda)\, \mathrm{d}\lambda \Big|
\end{aligned}
\tag{6}
$$

Earlier, detector outcomes $A(\alpha,\, \lambda)$, and $B(\beta,\, \lambda)$ were defined to be ± 1. From this, the following can be determined in (7).

$$
[1 \pm A(a',\, \lambda)\, B(b',\, \lambda)]\, p(\lambda) \;\geq\; 0 \quad \textit{and} \quad [1 \pm A(a',\, \lambda)\, B(b,\, \lambda)]\, p(\lambda) \;\geq\; 0 \tag{7}
$$

(7) allows the terms within the absolute values on the RHS of (6) to be separated, as shown in (8).

$$
\begin{aligned}
|E(a,\, b) \,-\, E(a,\, b')| \;\leq\; & \int |A(a,\lambda)\, B(b,\lambda)|\, |[1 \pm A(a',\lambda)\, B(b',\lambda)]\, p(\lambda)\, \mathrm{d}\lambda| \\
& + \int |A(a,\lambda)\, B(b',\lambda)|\, |[1 \pm A(a',\lambda)\, B(b,\lambda)]\, p(\lambda)\, \mathrm{d}\lambda|
\end{aligned}
\tag{8}
$$

As a result of the definitions of detector values mentioned earlier, it can also be determined that $|A(\alpha,\, \lambda)\, B(\beta, \lambda)| \leq 1$. Therefore the RHS of (8) must be less than or equal to the RHS of (9).

$$
\begin{aligned}
|E(a,\, b) \,-\, E(a,\, b')| \;\leq\; & \int [1 \pm A(a',\, \lambda)\, B(b',\, \lambda)]\, p(\lambda)\, \mathrm{d}\lambda \\
& + \int [1 \pm A(a',\, \lambda)\, B(b,\, \lambda)]\, p(\lambda)\, \mathrm{d}\lambda
\end{aligned}
\tag{9}
$$

It is important to observe that only $|A(a,\, \lambda)\, B(b,\, \lambda)|$ and $|A(a,\, \lambda) B(b', \lambda)|$ were removed. This is because these detector configurations were already present on the LHS inside the E expressions, thus being

redundant.

It is established that $\int p(\lambda)\,\mathrm{d}\lambda = 1$, as it is a normalized probability distribution. Therefore the $\int 1 * p(\lambda)\,\mathrm{d}\lambda$ terms in (9) can be factored and evaluated as shown in (10).

$$|E(a,\, b) - E(a,\, b')| \leq 2 \pm [\int A(a',\, \lambda)\, B(b',\, \lambda)\, p(\lambda)\,\mathrm{d}\lambda + \int A(a',\, \lambda)\, B(b,\, \lambda)\, p(\lambda)\,\mathrm{d}\lambda\,] \tag{10}$$

Referring to (1) for the previous definition, the RHS of (10) can be re-written in terms of $E(\alpha, \beta)$, as shown in (11).

$$|E(a,\, b) - E(a,\, b')| \leq 2 \pm [\,E(a',\, b') + E(a',\, b)\,] \tag{11}$$

The inequality in equation (12) is the most challenging version to violate experimentally, but it also ensures more reliable and credible results. This is because maximizing the right-hand side of equation (11) leads to a stronger constraint on the existence of hidden variables.

$$|E(a,\, b) - E(a,\, b')| \leq 2 + |E(a',\, b') + E(a',\, b)| \tag{12}$$

The rightmost term of (12) is subtracted over as shown in (13).

$$|E(a,\, b) - E(a,\, b')| - |E(a',\, b') + E(a',\, b)| \leq 2 \tag{13}$$

The LHS of (13) is represented by the letter S and has no physical meaning. (14)

$$S = |E(a,\, b) - E(a,\, b')| - |E(a',\, b') + E(a',\, b)| \tag{14}$$

The result is the famous "Bell's Inequality" displayed in (15).

$$S \leq 2 \tag{15}$$

The maximum constraint for probability correlations, including a hidden variable, is expressed by equation (15). However, it is crucial to note that the value of S can also be determined using a purely quantum mechanical approach as will be demonstrated in the following section.

To begin, we will establish the four bases to use when measuring the polarization of photons with polarizers A and B.

$$|V_\alpha\rangle = cos(\alpha)\,|V\rangle - sin(\alpha)\,|H\rangle \quad and \quad |H_\alpha\rangle = sin(\alpha)\,|V\rangle + cos(\alpha)\,|H\rangle$$

$$|V_\beta\rangle \,=\, cos(\beta)\,|V\rangle \,-\, sin(\beta)\,|H\rangle \quad and \quad |H_\beta\rangle \,=\, sin(\beta)\,|V\rangle \,+\, cos(\beta)\,|H\rangle$$

Where $|V\rangle$ and $|H\rangle$ represent horizontal and vertical polarization states for the signal and idler photons.

The state of the entangled photons is represented in equation (16), with the subscripts s and i denoting signal and idler, respectively.

$$|\psi\rangle \,=\, \frac{1}{\sqrt{2}}(\,|V_i\rangle\,|V_s\rangle \,+\, |H_i\rangle\,|H_s\rangle) \tag{16}$$

Using the four bases and the entangled state expression (16), we can compute the probability of coincident detection for every pair of polarization angles, as illustrated below.

$$P_{VV}(\alpha,\beta) \,=\, |\,\langle V_\alpha|_s\,\langle V_\beta|_i\,\psi\rangle\,|^{\,2} \,=\, \frac{1}{2}\,cos^{\,2}(\beta \,-\, \alpha)$$

$$P_{HH}(\alpha,\beta) \,=\, |\,\langle H_\alpha|_s\,\langle H_\beta|_i\,\psi\rangle\,|^{\,2} \,=\, \frac{1}{2}\,cos^{\,2}(\beta \,-\, \alpha)$$

$$P_{VH}(\alpha,\beta) \,=\, |\,\langle V_\alpha|_s\,\langle H_\beta|_i\,\psi\rangle\,|^{\,2} \,=\, \frac{1}{2}\,sin^{\,2}(\beta \,-\, \alpha)$$

$$P_{HV}(\alpha,\beta) \,=\, |\,\langle H_\alpha|_s\,\langle V_\beta|_i\,\psi\rangle\,|^{\,2} \,=\, \frac{1}{2}\,sin^{\,2}(\beta \,-\, \alpha)$$

It is important to mention these simplifications can only be made under the special conditions of an incident beam polarized to $\theta \,=\, \frac{\pi}{4}$ and the phase angle $\phi \,=\, 0$ or $\phi \,=\, \pi$. The above coincidence probability expressions can be plugged in to find $E(\alpha,\,\beta)$ as defined in (1); which, after some manipulation, can be reduced to the form found in (17).

$$E(\alpha,\,\beta) \,=\, cos[\,2(\beta \,-\, \alpha)] \tag{17}$$

It is then possible to calculate S (14), which is found to have a maximum theoretical value of $2\sqrt{2}$ at an angle differential of $\beta - \alpha \,=\, \frac{\pi}{8}$. This is in clear violation of the previous maximum classical constraint. (15) The significance of this conclusion cannot be overstated, as it provides evidence that the Theory of Hidden Variables cannot be a an interpretation of quantum mechanics, since the predictions of the two theories are inconsistent.

Applying (18) to the expression for $E(\alpha,\,\beta)$ (1) results in an equivalent expression for $E(\alpha,\,\beta)$ (19), that can be determined through experimentation.

$$P_{VV}(a,\,b) \,=\, \frac{N_{VV}(a,\,b)}{N_{TOT}} \tag{18}$$

$$E(a,\,b) \,=\, \frac{N(a,\,b) \,+\, N(a_\perp,\,b_\perp) \,-\, N(a,\,b_\perp) \,-\, N(a_\perp,\,b)}{N(a,\,b) \,+\, N(a_\perp,\,b_\perp) \,+\, N(a,\,b_\perp) \,+\, N(a_\perp,\,b)} \tag{19}$$

a, and $a_\perp$ are perpendicular angles of polarizer A, equivalent to detector modes capable of detecting vertically and horizontally polarized photons at the same efficiency respectively. The same applies for b and $b_\perp$ for polarizer B.

4 Methods

4.1 Initial Setup

This section will include details regarding construction of the setup before the experimentation procedure begins.

4.1.1 Overview

Figure 2 shows a diagram of the initial experiment setup.

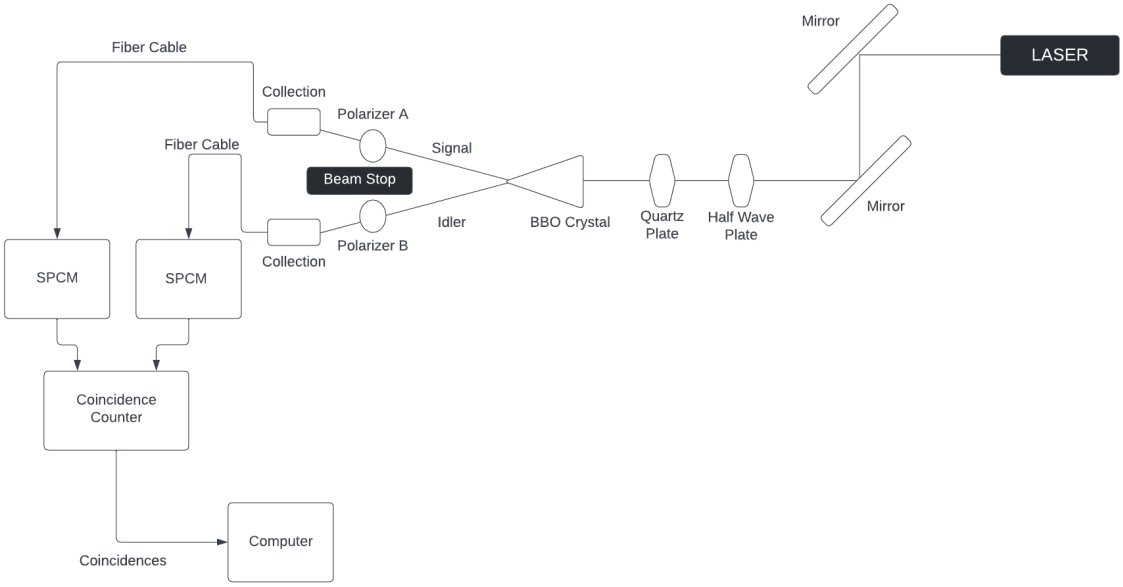

Figure 2: Experiment Setup

An overhead view of the construction of the setup is shown in figure 3.

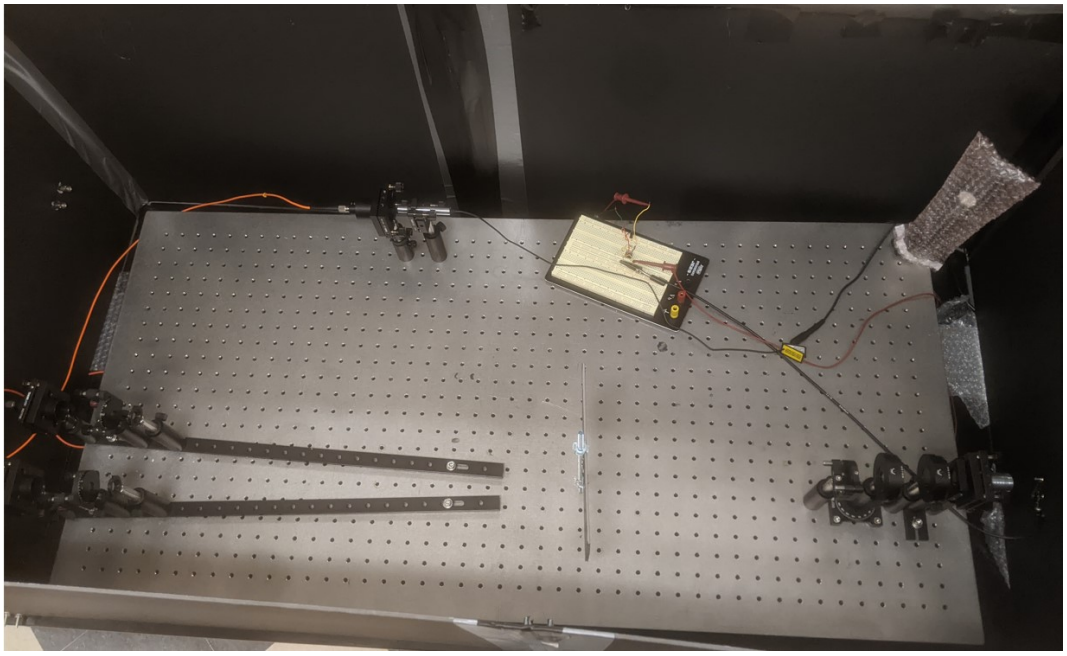

Figure 3: Experiment Construction

4.1.2 The 405 nm Laser

The laser utilized is a diode excavated from a Blue-Ray disc burner drive. This diode is powerful, capable of producing up to 900 mW of power when supplied with enough current. However, 100 mW of laser power should be sufficient for generating adequate photon pairs per second using the BBO crystals. The diode is installed into a heat sink before mounted to the board. This laser diode was chosen due to its affordability and recommended by Prutchi [1] as a viable alternative to more expensive options.

For powering the laser we are using a simple laser driver circuit built on a miniature breadboard. These circuits are designed to provide a constant current to the diode, making use of the LM317 constant voltage regulator. Regulated current provided to the diode is essential as the resistance of the diode will decrease over time as the diode heats up. This will result in the diode drawing more current until damage is caused if connected to an unregulated current supply.

The driver is designed to provide close to the minimum current needed for the diode to lase, which is 58 mA. For aligning and testing purposes, there is no need for an increase in power. A diagram of the circuit design is shown in figure 4.

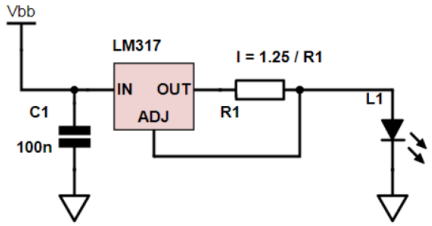

Figure 4: Laser Driver Circuit

The laser driver is powered using a 9V battery, and uses a 200 ohm resistor (R1) to get the desired current. The capacitor (C1) is 100 nF and the load resistance (L1) is our laser diode.

4.1.3 Beam dump

The experiment's beam dump follows the design Prutchi employed in his experiment. Figure 5 displays the construction.

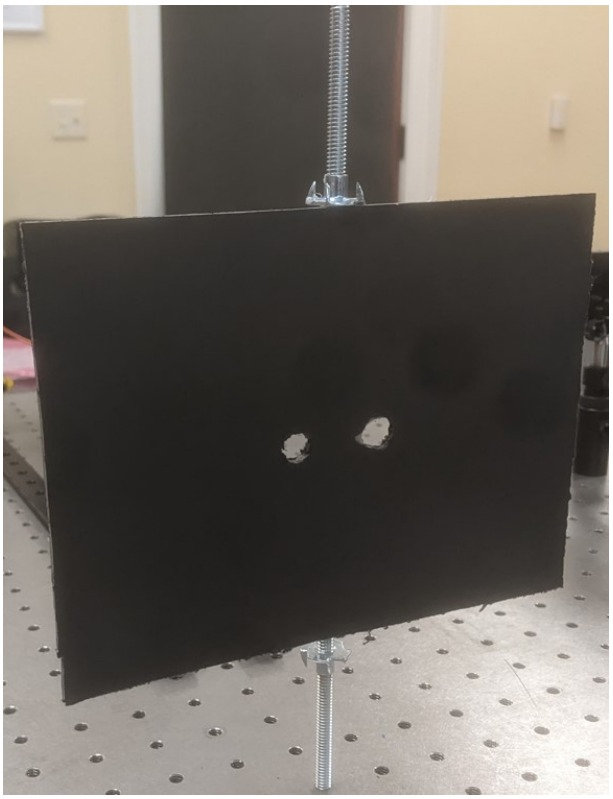

Figure 5: Beam Dump

The beam dump is made from a panel of black foam board measuring 6 inches in height and 8 inches in width. The foam board is fastened to a 1/4 inch threaded rod using a combination of hot glue and two t-nuts. Designed to be placed 12 inches away from the BBO crystals along the beam path, it features two 3/8 inch drilled holes at ± 0.64 inches from the center allowing the entangled photons to pass through. The remaining portion of the foam board will block the pump beam as well as any unrelated photons traveling different paths.

4.1.4 Alignment

Pre-BBO

To begin the alignment procedure special consideration must be taken for laser safety. The pump laser is, at minimum, a class 3b laser and therefore laser safety must be considered whenever turning this laser on. One should not attempt to align such a laser without proper laser safety training. We worked with our capstone advisor Dr. David Gore who is a certified optics professional when aligning the pump laser beam. The beam path is first simulated using a visible 5 mW laser pointer. A laser card is then used to assist in alignment for the 405 nm laser as the beam is very difficult to see when wearing protective eye wear. As our high powered laser had a quickly diverging beam, we decided to omit the alignment mirrors which were originally purposed with lengthening the beam path if necessary, and instead shortened the path as much as was feasible.

It is also important if working in a room with windows that the windows are covered with a non-reflective surface, we used a black foam.

The Pre-BBO alignment procedure was simple as we required a short beam path. All optical components including the laser were placed linearly. First the laser pump height is measured, and all other components on the table were set so their centers are level with the height of the pump laser beam. We used the pump laser beam height as our reference because it has to shortest range of movement vertically, however any piece can be used as the initial reference point. We used an iris to help center the beam incident on the BBO crystals.

Post BBO

Before any laser alignment takes place, the optical rails themselves must be oriented along the $\pm$ 3° paths from the pump laser. A right triangle can be constructed between the optical rail, the pump beam path, and the distance between the optical rail and the pump beam path. Simple trigonometry can be used to solve for the distance between the optical rail and the pump beam path at any distance along the beam path considering the angle of emitted entangled photons is known. The trigonometric relation of this right triangle is shown below.

$$tan(\theta_{from\,beam}) = \frac{x}{y} \tag{20}$$

Where θ is the angle between the optical rail and the pump beam path, y is the distance along the pump beam path from the BBO crystals, and x is the distance between the optical rail and the pump beam path completing the right triangle. As we had a sufficiently sized breadboard, we had the convenience of choosing two y distances, y_1 and y_2 such that x distances, $x_1 = 1$ inches and $x_2 = 2$ inches were multiples of 1. These were $y_1 = 19$ inches, and $y_2 = 38$ inches. It was necessary to mount each optical rail at two points so they are aligned with the $\pm 3°$ paths originating from the center of the BBO crystals. Thus we pre-aligned the rails with an error less than 0.3%.

After the rails have been aligned, each rail had three components mounted in this order. An iris, a linear polarizer, and a collector assembly. A picture of one of our rails is shown in Figure 6.

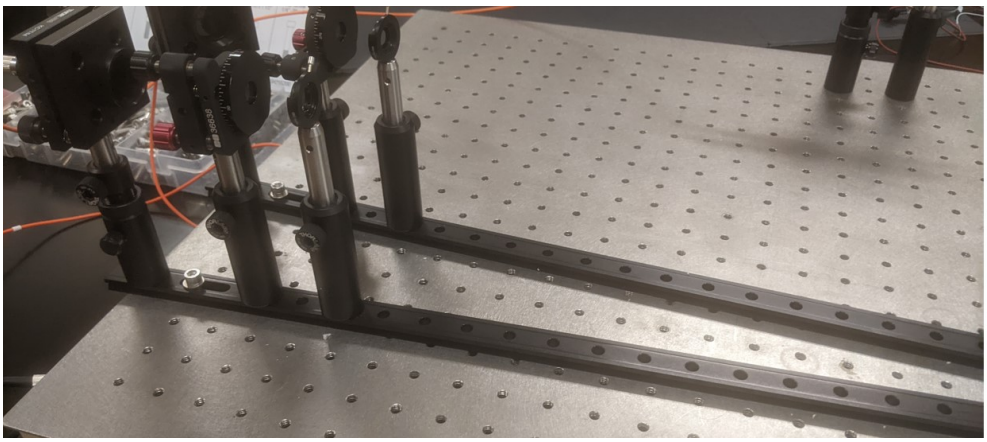

Figure 6: Rail Assembly

The alignment procedure began with first removing the long-pass filters from the collector assemblies, then projecting a visible 5 mW laser backwards from the position of one of the photon collecting heads of the SPCM's onto the crystals. This required a third collector assembly to couple the 5 mW laser into the fiber. Figure 7 shows the setup for the backwards projected laser.

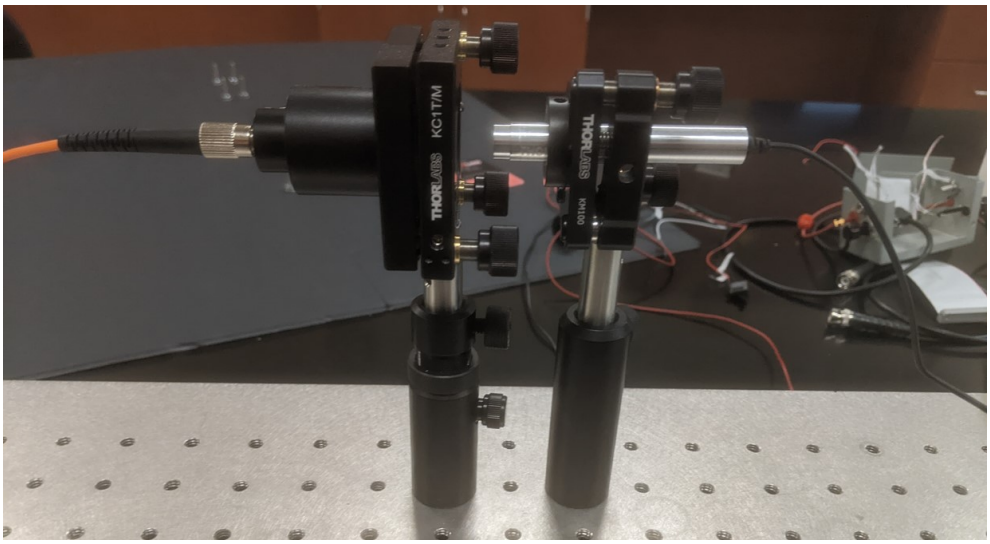

Figure 7: Backwards Projected Laser

Small angular adjustments must be made using the precision mounts of the collector assemblies until the backwards projected beam is incident upon the crystals. The crystals were then removed, placed in a bag with a silica dessicator, and a suitable mirror for the wavelength of the visible 5 mW laser was placed in its mount. The collector assembly on the opposite rail was then adjusted until the reflected laser from the mirror coupled into the fiber cable of the opposite end and could be seen exiting the fiber in the position of the opposite SPCM photon collecting head.

It is important to mention a step is needed to verify alignment after placing the long pass filters back into the collector assemblies, this will be discussed in the section at the end of the paper.

4.1.5 Collector Assembly

The collector assembly is an optical tube mounted upon a translating kinetic mount containing a long-pass filter and fiber collimating lens. This aperture is responsible for guiding the beam of entangled photons into fiber optic cables which are connected to the Single Photon Avalanche Diodes (APDs). The translating kinetic mount allows for fine adjustments of the fiber coupling lens, and the 780 nm long-pass filter helps protect the APDs from overload by blocking any photons from the diverging pump laser that may end up along the same path as the entangled photons. A diagram of the collector assembly is shown below in Figure 8.

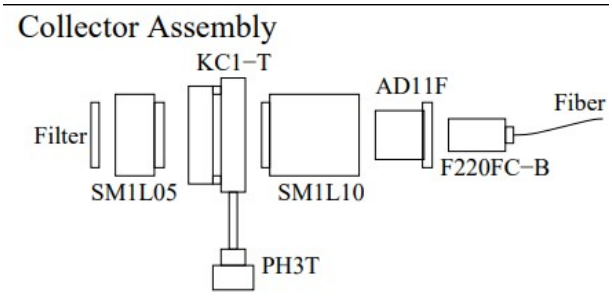

Figure 8: Collector Assembly

4.1.6 APDs and Coincidence Counter

The APDs and Coincidence Counter make up the apparatus that outputs counts of detected photon pairs over a period of time to a computer. The fiber optic cables from the collector assembly are connected to the sensors on the APDs. Each APD produces a 2.2V voltage pulse 10 ns in length when a photon is detected within its frequency range. These voltage pulses are then terminated into 50Ω and transferred into pins on the external GPIO header of the Altera DE2-115 field programmable gate array (FPGA) programmed to act as a coincidence counting unit. The FPGA communicates with a computer using an RS232 cable and LabVIEW software. This is a summary of the apparatus responsible for making usable data from the entangled photon pairs, the process of construction and each part is explained in greater detail in the following sections.

Signal Receiving Box

The function of the signal receiving box is straightforward. It is a container created to transmit the signals from the APDs to the coincidence counting FPGA. The APD signals must be properly terminated in 50Ω to avoid signal rebound according to the user manual. A diagram for terminating the signal is shown in figure 9.

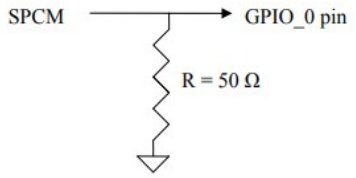

Figure 9: Signal Termination

Regarding the construction of the signal receiving box, we used black foam board secured with hot glue. We originally attempted using a metal box, but had difficulty drilling adequate sized holes into it. The FPGA is capable of counting up to four way signal overlaps so four holes are drilled into the box. In each hole a female to male BNC converter is inserted with the female side on the outside of the box. The APD output pulses Each BNC connector has a wire from a ribbon cable soldered to the male pin on the inside. These wires carry the signals from the four signal sources (APDs) into the pins on the GPIO header of the FPGA.

The signals must be transmitted to specific pins on the FPGA because of how it is programmed. The GPIO configuration for the Altera DE2-115 is shown in Figure 10. It is also wise to ground the remaining unused pins, this will be discussed in the section for continued work on the experiment as it has not yet been

completed.

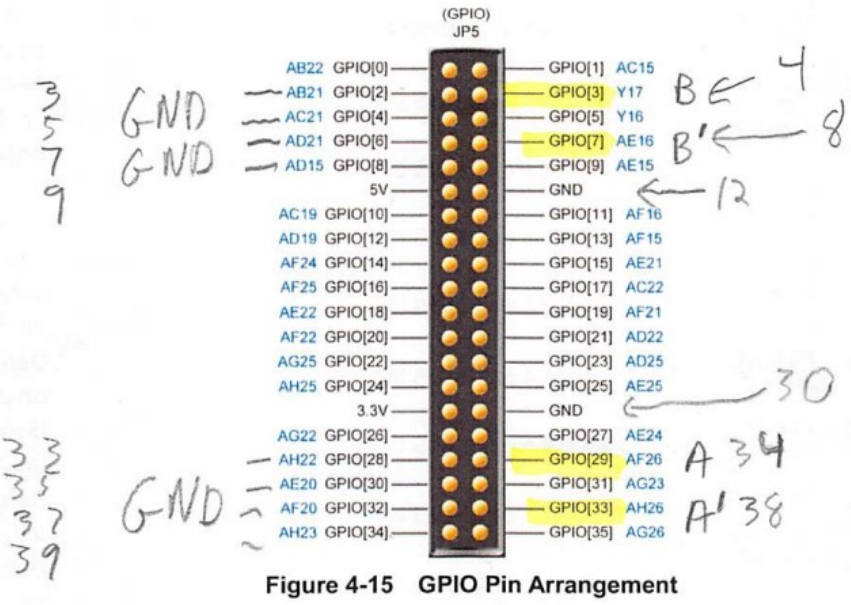

Figure 10: Pin configuration

The Coincidence Counting Board

The Altera DE2-115 is programmed using software developed by the University of Berkeley off the work that was performed by Jesse Lord at Reed College. [9] The coincidence counting unit (CCU) is capable of receiving inputs from a maximum of four detectors. Additionally, it is equipped with eight 32-bit counters, which can be utilized to keep track of four individual single counts, as well as four coincidences of 2, 3, or 4-fold nature (dependent on the switch settings). The software to program the board comes in a pre-compiled format, and can be installed to the board using Intel Quartus. It is important not to recompile the software upon loading Quartus. Ensuring the board is properly connected to the computer, the process to program the board should be as simple as clicking the "program" function in the Quartus software once the compiled project is selected. We ended up needing to program the board using a version of Quartus only available on Windows 7, as otherwise the programming step failed. We used a virtual machine running Windows 7 and the CD drive the board came with in order to download the appropriate version of Quartus. We are unsure if this is a typical requirement as it was not mentioned in the published instructions. Other than that potential hurdle installing the software is straightforward as it is already pre-compiled.

What is not included with the board is LabView software to interact with the board in order to output recorded data to file, as well as a software for performing the necessary calculations. This is further discussed in the ending section for continued work on the experiment.

4.1.7 Enclosing Box

It is important that the APDs are operated in complete darkness to ensure the sensors do not overload from ambient photons. One possibility is to prepare the room so that complete darkness is achieved, the other possibility is to enclose the setup within a box. As we cannot fully proof the room for complete darkness due to tall windows, we have chosen to enclose our setup within a light tight box. The setup placed within the box is shown in Figure 3.

For the construction of the box we used panels of black foam board secured by parallel brackets and L brackets. Cracks in sections where panels connected together were light proofed using a combination of black silicone sealant and electrical tape. Holes are drilled into the box for two BNC connectors inserted with which the APD signals will be transferred through. The connectors were secured using silicone sealant. Because our breadboard has adequate space we will simply be placing the APDs on its surface. However, it is a possible design if breadboard space is an issue to mount them to the side of the box. The lid of the box and the interlock mechanism is still under construction and will be discussed in the continued work section at the end of the paper.

5 Results and Analysis

As our apparatus is not yet capable of taking data, we have no experimental results. The further tasks necessary to be completed in order to achieve results and perform analysis will be discussed in the section for continued work.

6 Continued Work

As our experimental construction and execution of the experiment is not yet completed. This section will be devoted to providing instruction for remaining tasks to any interested future students.

6.1 Constructing the Box Lid

The lid of the box is assembled. However, it must still be attached to the frame of box. We left one side without foam padding as this is where we planned to attach it. The lid can be attached using the three purchased hinges and the bolts and nuts that came with them. After attaching the lid of the box it must be light-proofed in a manner that does not restrict motion of the lid. For this task we planned to cover the cracks using a black foam sheet secured onto the lid and the box itself, as we thought applying insulation directly to the cracks may restrict the motion of the lid.

6.2 Verifying alignment

Backwards projected alignment should be verified after the long-pass filters are inserted back into the collector assemblies. It is possible they may alter the beam path slightly, so the backwards projection procedure should be repeated using a 980 nm IR laser which will pass through the filters. It is important to order a laser powerful enough, we made the mistake of ordering a 1 mW 980 nm laser and it was barely visible after coupling into the first fiber cable. Prutchi references using a 30 mW 980 nm laser, so a laser of considerable power should be considered before purchasing. A viewing card will also be necessary to see the beam path, we have one purchased in the lab that works for both the pump beam as well as 980 nm. We have also purchased an appropriate mirror for reflecting the 980 nm beam.

6.3 Interlock

A switch with a lever must be secured to the side of the box. This switch will activate the laser when the box is closed, and deactivate when the lid is opened. Some kind of weight or attachment to the lid of the box may be necessary to achieve consistent behavior. This interlock is not only for the safety of anyone who happens to open the box without proper equipment, but also acts as a safety laser shutoff should the detectors start to overload. The switch is already purchased, it bridges two pins when the lever is pressed down. Routing the connection between the power source and the laser driver through the switch will result in a functioning interlock.

6.4 Experimental Laser Driver

For the purposes of performing the experiment, a different laser driving circuit ensuring maximum current stability must be constructed. Figure 11 shows a design used by Prutchi to drive their laser with a stable 160 mA to ensure near constant laser power output. As their diode may differ from ours, a power meter should be used to verify the power of the laser when driven by this circuit. The current delivered by the circuit can be adjusted by exchanging the resistors as according to the LM317 user manual.

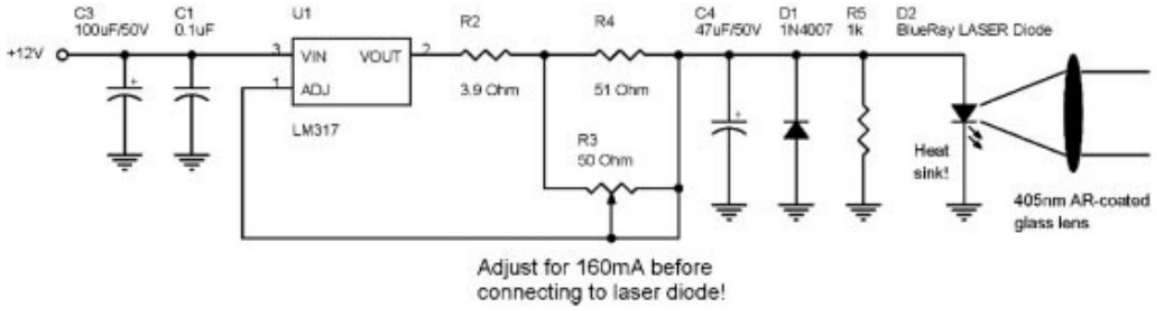

Figure 11: Driver Construction

6.5 New beam dump

For use with the pump laser powered with the new laser driver, it is a wise decision to revise the design of the beam dump. Instead of simply using a portion of the black foam board to eliminate the majority of the beam, a stack of razor blades should be inserted which has a lower reflectivity. The process may be as simple as taking the existing beam dump, excavating a hole in the center between the two holes, and securing a stack of razor blades there. Should the gap between the holes, 1.28 inches be too small to install the razor blades, an additional beam dump can be constructed to be placed further from the pump laser, thus having a larger separation between the two drilled holes allowing room for the razor blades to be installed. For example, a beam dump placed 19 inches from the crystals would have a separation of 2 inches between the centers of the drilled holes.

6.6 FPGA Software

It was previously mentioned that the FPGA would require a LabView interface in order to interact with it. Two layers to this interface are required. First is the monitoring layer, it is important to monitor the counts per second of each relevant counter to make sure the APDs are operating within safe thresholds. This would be the individual counts for both detectors, as well as the coincidence count. For the monitoring layer, a repeating loop will need to zero the selected counters every second, and display the values to the screen.

The second layer to this interface is the usability layer. Data from this experimental procedure is taken in the form of counts per unit of time, and is usually averaged over a number of data trials. For example, when calculating the resulting constraint, coincidence counts per every 0.5 seconds are averaged over 10 trials. Similar procedures are used for recording counts when calibrating various optical components such as the quarter wave plate. At the press of a button, this layer should zero the counter value, wait a specified period of time, and then store the relevant counter values into an array which is written to a csv file. A python for loop can be embedded into the LabView to repeatedly perform this procedure to record data over a desired number of trials. I am unsure of whether it would be easier to write all of the data from each trial to the file directly, and perform the averaging and processing afterwards. Or if it is possible to store the data in some sort of integer array, calculate the average of that array, and only output that value to the file. For references, there are included libraries of LabView interface example tutorials included with the

DE2 board software from Whitman. There are also a number of LabView interface files included with the DE2-115 board software from the University of Berkeley. I recommend using the tutorial from Whitman as well as the DE2-115 interface files as a guide for writing your own.

6.7 Data Analysis

The software for the data analysis will need to be formatted in order to process the data output by the LabView interface. I recommend using Python as it is simple to read in data from a list of CSV files. Once all of the counts are read in, the count values from each experiment must be used to calculate E values for each experimental configuration as shown in Equation (19). I suggest a design where counts from each configuration of polarizers are stored in separate CSV files. This will result in 16 total CSV files that can be named to represent the data they hold. This will make separating the count values into their specific categories very simple when reading in the data.

6.8 Calibration Procedures

This sub-section will discuss the calibration procedures for alignment of various components. These calibration procedures must take place before the experiment is performed to ensure a maximally entangled photon pair state.

6.8.1 Linear Polarizer

The linear polarizer in the Pre-BBO section will need to be calibrated to an orientation of 45° with respect to the BBO crystals. A simple procedure could be to simply rotate the crystals until a maximized coincidence count is achieved. However, a more involved and thorough process would be to orient the polarizer at 45° with respect to the vertical, and then rotate the crystals afterwards to maximize the output. This will require a collimated beam with known polarization (ideally vertical), an additional linear polarizer in a rotating mount, and a power meter to ensure as the polarizers are rotated with respect to one another a maximum and minimum beam power are recorded accurately. There are several tutorials on Youtube for performing this procedure, including one made by Thorlabs.

6.8.2 Quarter-Wave Plate

The quarter wave plate induces a phase shift in the light passing through it. There is a phase shift introduced in the output of the pair of BBO crystals due to them being mounted side by side a finite distance from each other. To maximize the entangled state, the phase shift introduced by the BBO crystals must be minimized, this can be visualized as overlapping their conical outputs. This is achieved in practice by introducing a phase shift using the quarter-wave plate that minimizes the phase shift of the BBO crystals. The magnitude of the phase shift is determined by the orientation of the quartz plate along the vertical and optical axes. Minimizing the BBO crystal's phase shift is not an exact science, so we will find the optimal alignment experimentally.

We will start with the plate oriented vertically (0°) in the optical plane, and gradually rotate the BBO crystal in the horizontal plane. Then, we will plot coincidence curves at different polarization angles of the linear polarizers along the optical rails. The angles chosen should have equivalent coincidence counts in a theoretically maximized entangled state. In an experimental setting, a perfect maximally entangled state is difficult to achieve, the goal is to be as close as possible. The ideal alignment is the angle where the coincidence curves come closest to intersecting one another. An example graph is shown in figure 12.

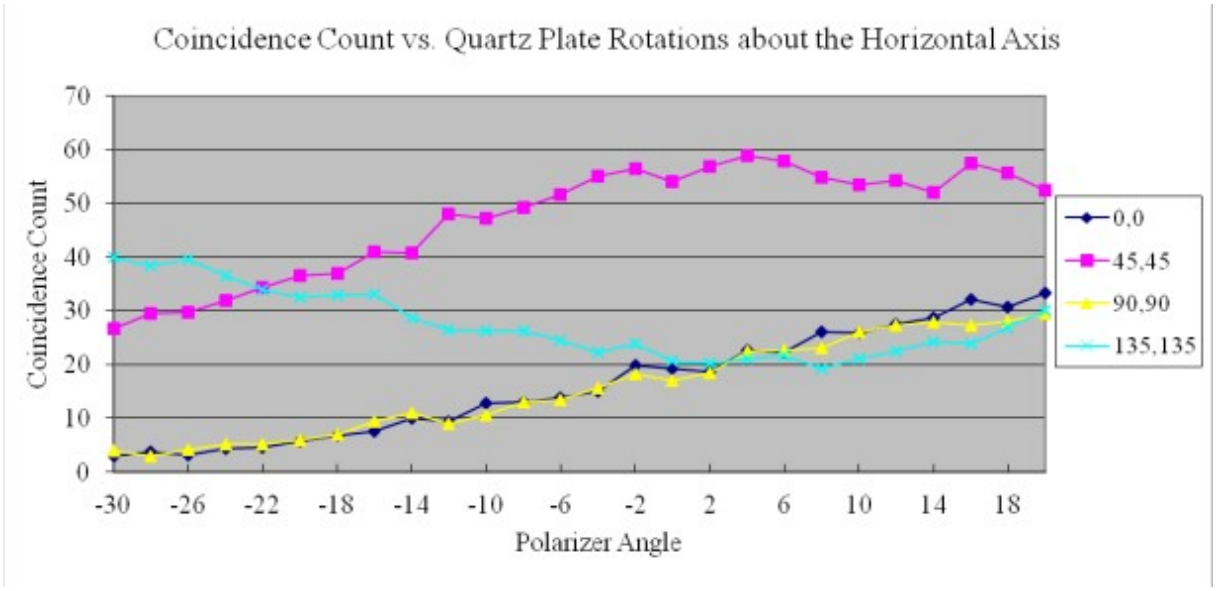

Figure 12: Pin configuration

Once the optimal horizontal angle has been found, the process will be repeated to align the quarter-wave plate along the optical plane. We will leave the quarter-wave plate at the optimal horizontal alignment, and gradually rotate the BBO crystal in the optical plane. The same procedure for the optical axis is highlighted in figure 13.

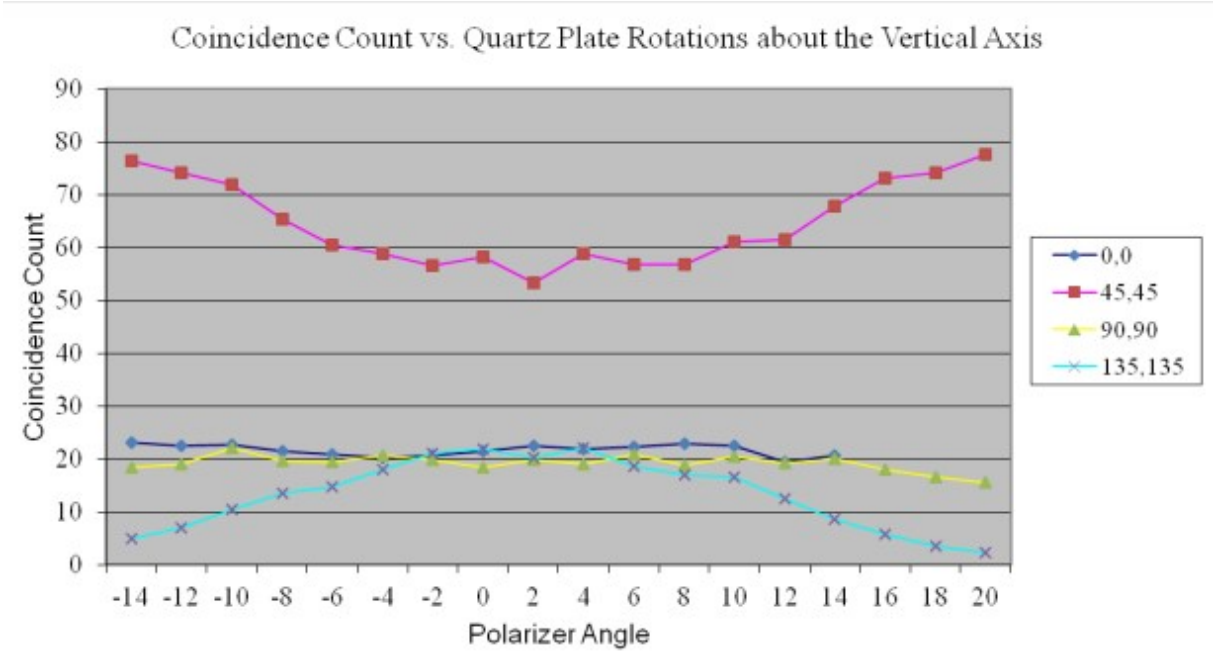

Figure 13: Pin configuration

6.8.3 BBO Crystals

It is important to mention that Dr. Lukishova [4] has instructions in her lab for a procedure maximizing the output of the APDs through alignment along the optical axis. An EM-CCD camera with an interference

filter placed at the camera entrance can be used to observe the conical output of entangled photons from the BBO crystals. The BBO crystals may be rotated around the optical axis until the output cone seen through the EM-CCD camera is brightest. An image of the observed output is shown below in figure 11.

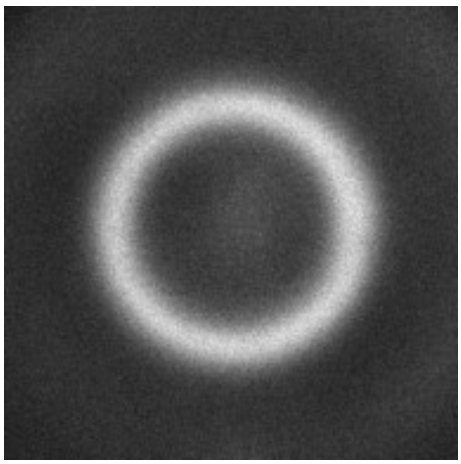

Figure 14: Pin configuration

This alignment procedure of the APDs may be necessary as the crystals are removed from their mount and replaced by hand when aligning the backwards projected lasers, which may result in some error of orientation.

6.8.4 Re-Calibration of Alignment

In reading the lab reports of Dr. Lukishova's students, as well as the lab manual of this experiment. It is apparent that proper alignment of this apparatus is elusive. It is mentioned in multiple reports where initial results were subpar that improvement was made after re-aligning the apparatus. Both Prutchi and Dr. Lukishova recommend including extra lenses before repeating the alignment process should this be an issue. The primary mentioned spot is a lens in front of the BBO crystals precisely focusing the laser light onto them. This ensures a maximized production of entangled photon pairs per unit of laser power and may also reduce divergence of the pump laser into the paths of the entangled pairs.

References

[1] D. Prutchi and S.R. Prutchi, in "Exploring Quantum Physics through Hands-on Projects" (Wiley, Hoboken, NJ, New Jersey, 2011), pp. 211–226.

[2] N. Cothard and P. Heuer, in "Observing Entanglement: Violations of Bell Inequalities" (University of Rochester, NY, New York, 2013)

[3] B. Betchart, in "A Test of Bell's Inequality for the Undergraduate Laboratory" (Oberlin College, OH, Ohio, 2004)

[4] S. Lukishova, in "Lab 1. Entanglement and Bell's Inequalities" (University of Rochester, NY, New York, 2008)

[5] C. Marsh, G. Jensen, S. To, in "Entangled Photons and Bell's Inequality" (University of Rochester, NY, New York, 2013)

[6] Einstein, A., Podolsky, B., Rosen, N. (1935). Can Quantum-Mechanical Description of Physical Reality be Considered Complete? Physical Review, 47(10), 777-780.

[7] Bell, J. S. (1964). On the Einstein Podolsky Rosen paradox. Physics Physique , 1(3), 195-200.

[8] Clauser, J. F., Horne, M. A., Shimony, A., Holt, R. A. (1969). Proposed experiment to test local hidden-variable theories. Physical Review Letters, 23(15), 880-884.

[9] "Coincidence Counting Units." Coincidence Circuit, http://people.reed.edu/ beckm/QM/circuit/circuit.html.